ELSEVIER

Journal of Structural Geology 30 (2008) 622–632

JOURNAL OF STRUCTURAL GEOLOGY

www.elsevier.com/locate/jsg

Relationships between faults, extension fractures and veins, and stress

T.G. Blenkinsop*

School of Earth and Environmental Sciences, James Cook University, Townsville, Qld 4811, Australia

Received 22 May 2007; received in revised form 14 January 2008; accepted 15 January 2008
Available online 25 January 2008

Abstract

Faults are commonly related to extension fractures, defined here as including extension veins. Extension fracturing is integral to fault initiation and propagation, and extension fractures also form after fault slip. In these situations, fault planes contain the intermediate principal stress $\boldsymbol{\sigma}_2$, and slip is perpendicular to the line of intersection between the fault and the extension fractures. However, for reactivated faults, multiple fault sets, and faults formed according to the Healy theory, $\boldsymbol{\sigma}_2$ is not necessarily within the fault plane. A theoretical analysis shows that the trace of an extension fracture on a fault can make angles from 0° to 90° with the maximum resolved shear stress. The angle depends on the fault orientation relative to the principal stresses, and the ratio between the stresses. Extension fractures only intersect faults perpendicular to the maximum resolved shear stress on faults containing the maximum or intermediate principal stresses, or when their magnitudes are equal ($\sigma_1 = \sigma_2$). Field observations show that extension fractures can intersect faults along lines at oblique angles to slip directions, as predicted by the theory. Such angles may be indicators of fault reactivation, multiple sets of faults, or Healy theory faulting.

Keywords: Fault; Slip; Extension fracture; Vein; Stress; Dynamic analysis

1. Introduction

Extension factures and veins are commonly found adjacent to faults (e.g. Fig. 1) and within fault zones at a range of scales. ''Extension fractures'' will be used subsequently to refer to fractures and veins with a dominantly extensional (mode I) displacement. In many cases of extension fractures observed around faults in the field, compelling arguments show that extension fractures formed synchronously with slip on associated faults. Experiments demonstrate that extension fracturing is integral to fault initiation and propagation (e.g. Paterson, 1978).

Several models have been proposed to account for geometrical and temporal relations between faults, coeval extension fractures, and principal stresses (e.g. Wilson et al., 2003; Crider and Peacock, 2004). In most models, the fault plane is considered to contain the intermediate principal stress axis, and extension fractures intersect the fault along lines perpendicular to the slip vector of the fault, which is consistent with the intermediate stress having no influence on the fault slip direction.

However, other possibilities exist for the geometric relationships between extension fractures and faults because of fault reactivation, multiple fault sets, and faults formed by the Healy theory (Healy et al., 2006). The aim of this paper is to develop a general theoretical basis that encompasses all of these possibilities, and can be supported by field examples.

2. A review of models for relationships between faults and extension fractures

2.1. Introduction

Five different approaches to understanding relationships between faults and extension fractures can be identified (Table 1, Fig. 2). These approaches deal with extension fractures that formed before, during or after fault propagation within the same deformation event. The concepts of pre-existing and precursory structures (Crider and Peacock, 2004) are most useful in this context: a pre-existing structure is one formed in an

* Tel.: +61 7 4728 5915; fax: +61 7 4725 1501.
E-mail address: thomas.blenkinsop@jcu.edu.au

0191-8141/$ - see front matter © 2008 Elsevier Ltd. All rights reserved.
doi:10.1016/j.jsg.2008.01.008

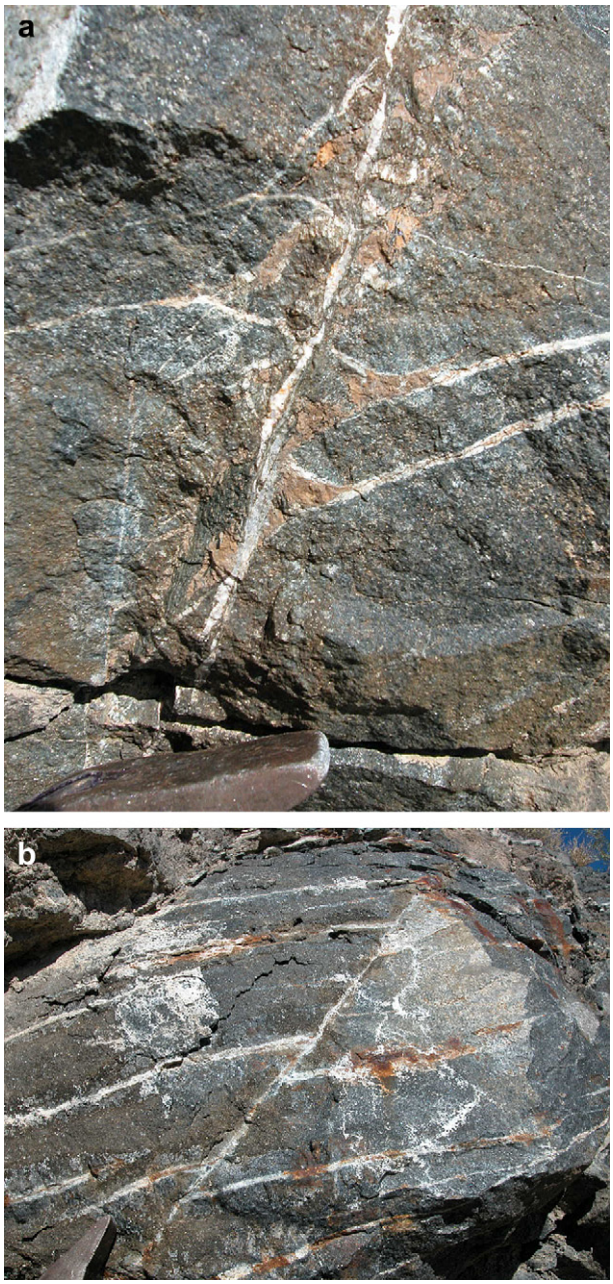

Fig. 1. Extension veins associated with reverse faults. Scapolite veins in an amphibolite in the Eastern Fold belt of the Mount Isa Inlier (UTM Zone 54K, 0416079 7703159). Note reverse separation of veins in both photographs. Slight curvature of veins is interpreted as drag in (a). Photographs look due south and show east over west reverse movement, likely to have occurred during D2 of the Isan Orogeny at ~1600–1580 Ma. Hammerhead for scale approximately 10 cm long.

earlier stress field, unrelated to faulting, and a precursor structure is one that forms during the early stage of faulting in the same stress field. The principal stress vectors are $\boldsymbol{\sigma}_1$, $\boldsymbol{\sigma}_2$, $\boldsymbol{\sigma}_3$, with magnitudes $\sigma_1 \geq \sigma_2 \geq \sigma_3$, taking compression positive.

2.2. Extension fractures as pervasive precursors to faults

Extension fractures are perhaps most commonly understood to have formed pervasively in a rock as precursors to faulting (Fig. 2a). This evolution is strongly supported by experiments (e.g. Brace et al., 1966; Brace and Martin, 1968; Scholz, 1968; Paterson, 1978; Peng and Johnson, 1972; Rutter and Hadizadeh, 1991) and microstructural observations from natural faults (e.g. Engelder, 1974; Blenkinsop and Rutter, 1986). Fractures link and coalesce to form a fault zone, which they intersect along a line perpendicular to the slip direction. The extension fractures considered in most of these studies are microscopic, but on a larger scale, joints and veins have been identified as precursors to faulting (e.g. Martel et al., 1988; Peacock and Sanderson, 1992, 1995a,b; Willemse et al., 1997; Mollema and Antonellini, 1999; Acocella et al., 2003). Faulting may also evolve by localisation of joints or veins into en echelon arrays (Olson and Pollard, 1991; Smith, 1996; Teixell et al., 2000).

2.3. Extension fractures that propagate from the tips of fractures loaded in shear

Experiments show that extension fractures form at the tips of isolated fractures or flaws that have been loaded in shear (e.g. Brace and Bombolakis, 1963; Tapponier and Brace, 1976). The formation of such "wing cracks" (Fig. 2b) is well understood from a theoretical point of view (e.g. Horii and Nemat-Nasser, 1985; Pollard and Segall, 1987; Cooke, 1997; Willemse and Pollard, 1998), and natural examples of wing cracks (and similar features such as tail cracks, pinnate and feather fractures) have been described (e.g. Rispoli, 1981; Engelder, 1989; Kattenhorn and Marshall, 2006). Faulting may occur by the linkage of wing cracks, that are themselves formed by slip on pre-existing fractures or flaws (e.g. Segall and Pollard, 1983; Horii and Nemat-Nasser, 1985; Granier, 1985; Kemeny and Cook, 1987; Martel, 1990). Linking of fractures loaded in shear by wing cracks is one way to explain the apparent paradox that isolated shear fractures cannot grow by in plane propagation (e.g. Lawn and Wilshaw, 1975; Cox and Scholz, 1988; Petit and Barquins, 1988).

The concept that extension fractures propagate from the tips of fractures loaded in shear is in a sense the opposite of the first model, which posits that pervasive extension fracturing precedes fault localisation. In contrast, extension fractures in this case form after shear loading of fractures, and faults evolve by linkage of extension fractures, which propagate in the stress fields of overlapping fracture tips. Wing cracks are generally understood to intersect their parent fracture perpendicular to the slip direction, and the same relationship holds between wing cracks and faults.

2.4. Extension fractures localised in a fault process zone

In this view, fault propagation is preceded by or synchronous with localised extension fracturing in the process zone around the crack tip (Fig. 2c, e.g. Rudnicki, 1980; Reches and Lockner, 1994; Vermilye and Scholz, 1998). The process zone is the rock volume containing features that results from fault-tip propagation, as distinct from the damage zone that describes the body of rock containing all structures related to fault deformation

Table 1
Common relationships between extension fractures and faults

Relationship	Timing	Association	θ	Scale	References
Extension fractures as pervasive precursors to faults which form in a zone of linked fractures	1. Extension fractures 2. Faults	Faults link zone of extension fractures; also extension fractures elsewhere	90°, although many studies in 2D, and experiments are biaxial	Commonly observed microscopic-ally; also field studies on m scale	Brace et al., 1966; Brace and Martin, 1968; Engelder, 1974; Paterson, 1978; Peng and Johnson, 1972; Blenkinsop and Rutter, 1986; Martel et al., 1988; Olson and Pollard, 1991; Peacock and Sanderson, 1992, 1995a,b; Rutter and Hadizadeh, 1991; Scholz, 1968; Smith, 1996; Willemse et al., 1997; Mollema and Antonellini, 1999; Acocella et al., 2003; Teixell et al., 2000.
Extension fractures that propagate from the tips of fractures loaded in shear; wing cracks connect to form faults	1. Fractures 2. Extension fractures (wing cracks)/ flaws 3. Faults	Extension fractures at crack tips; faults link zone of cracks and extension fractures	90°, although many studies in 2D, and experiments are biaxial	Microscopic and mesoscopic	Brace and Bombolakis, 1963; Lawn and Wilshaw, 1975; Tapponier and Brace, 1976; Rispoli, 1981; Segall and Pollard, 1983; Granier, 1985; Horii and Nemat-Nasser, 1985; Kemeny and Cook, 1987; Pollard and Segall, 1987; Petit and Barquins, 1988; Cox and Scholz, 1988; Engelder, 1989; Martel, 1990; Cooke, 1997; Willemse and Pollard, 1998; Kattenhorn and Marshall, 2006
Extension fractures localised in a fault process zone	Extension fractures simultaneous with propagation	Extension fractures are localised around fault tip; may be left in a damage zone	90° assumed but oblique angles measured	Microscopic	Rudnicki, 1980; Blenkinsop and Drury, 1988; Scholz et al., 1993; Reches and Lockner, 1994; Anders and Wiltschko, 1994; Reches and Lockner, 1994; Cowie and Scholz, 1998; Vermilye and Scholz, 1998; Shipton and Cowie, 2001; Martel and Langley, 2006
Extension fractures formed after slip on irregular fault surfaces	1. Faults 2. Extension fractures	Extension fractures adjacent to faults	90°	Microscopic-mesoscopic	Friedman and Logan, 1970; Conrad and Friedman, 1976; McEwen, 1981; Teufel, 1981; Hancock and Barka, 1987; Chester and Fletcher, 1997; Chester and Chester, 2000; Wilson et al., 2003
Fault–fracture mesh	Cyclic failure modes	Pervasive network	90°	Microscopic–Mesoscopic	Hill, 1977; Sibson, 1996, 2004; Eichhubl and Boles, 2000; de Ronde et al., 2001; Tunks et al., 2004; Lafrance, 2004

The angle θ is the angle between the intersection of the extension fracture and the fault and the slip direction, Illustrated in Fig. 4b. See text for references.

(Vermilye and Scholz, 1998). In the process zone model, extension fracturing is not pervasive throughout the rock volume and the development of extension fractures interacts with fault propagation. This model is supported by experimental observations (Reches and Lockner, 1994), by field examples (Blenkinsop and Drury, 1988; Anders and Wiltschko, 1994; Vermilye and Scholz, 1998; Martel and Langley, 2006), and by theory (Cowie and Scholz, 1998; Shipton and Cowie, 2001). The process zone model combines elements of both the preceding models: fault propagation occurs by extension fracture linkage, but the extension fractures are localised by the propagating fault. Models for fracture orientations in the process zone suggest that extension fractures should intersect the fault plane perpendicular to the fault slip vector (e.g. Scholz et al., 1993).

2.5. Extension fractures formed after slip on irregular fault surfaces

Extension fractures that formed after a slip event on a fault have been observed in experiments on a microscopic scale (“microscopic feather fractures”; Friedman and Logan, 1970; Conrad and Friedman, 1976; Teufel, 1981). These microfractures occur only within grains adjacent to the fault, where they are commonly wedge-shaped towards the fault plane (Fig. 2d), and they are close or parallel to the direction of applied maximum principal stress. Extension fractures associated with slickensided surfaces between pebbles in a conglomerate (McEwen, 1981), and comb fractures (Hancock and Barka, 1987), may fall into this category. All these extension fractures are distinct from the three previous cases because they form after a finite slip, rather than during propagation. They can be explained and modelled as the effect of stress concentrations due to movement around fault bends or asperities (Fig. 2e) (Chester and Fletcher, 1997; Chester and Chester, 2000; Wilson et al., 2003). These extension fractures intersect the fault surface perpendicular to the slip direction.

2.6. Extension fractures and faults form a mesh

Faults and extension fractures may grow together and link to form a fault–fracture mesh (Fig. 2e; Hill, 1977; Sibson, 1996, 2004). In models and field examples of meshes, the

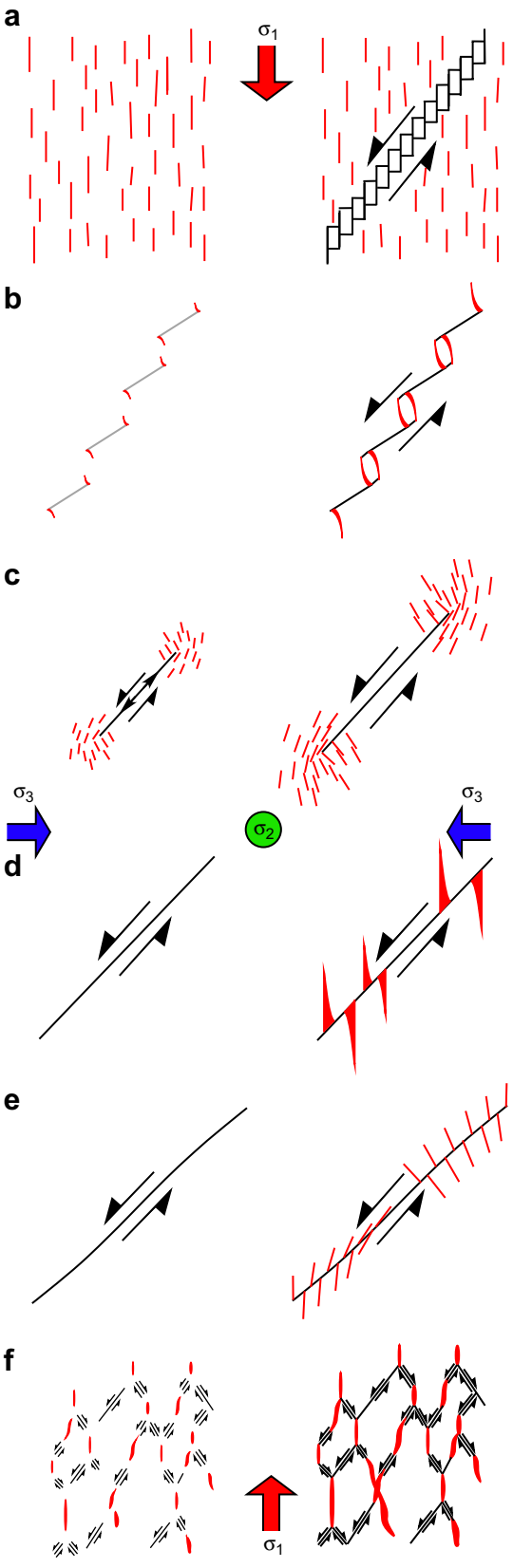

extension-fracture-fault intersection is assumed or interpreted to be parallel to $\boldsymbol{\sigma}_2$ and perpendicular to the fault slip direction (e.g. Eichhubl and Boles, 2000; de Ronde et al., 2001; Lafrance, 2004; Tunks et al., 2004).

2.7. Faults that do not contain $\boldsymbol{\sigma}_2$

The above models consider that extension fracturing and fault propagation occur in a single related deformation event. They assume or imply that faults contain $\boldsymbol{\sigma}_2$, and that the intersection between extension fractures and the fault will be perpendicular to the slip direction. However, at least three circumstances exist where these conditions may not apply. Firstly, during fault reactivation, which is commonly linked to extension fracturing, $\boldsymbol{\sigma}_2$ may not lie within the fault plane (Fig. 3a). This situation may apply to faults formed on pre-existing structures, which by definition formed in a different stress field from that of the fault (e.g. Cruikshank et al., 1991; Wilkins et al., 2001; Crider and Peacock, 2004).

An increasing number of studies recognise that multiple sets of faults can be formed in single deformation events in nature (e.g. Aydin and Reches, 1982; Oesterlen and Blenkinsop, 1995; Beacom et al., 1999; Crider, 2001; De Paola et al., 2005; Imber et al., 2005; Jones et al., 2005; Miller et al., 2007) and experiments (e.g. Oertel, 1965; Reches and Dietrich, 1983). Theoretical accounts for such geometries have been given by Reches (1978, 1983), Krantz (1988), and Johnson (1995). In these polymodal fault patterns that form in a single stress field, at least some faults cannot contain $\boldsymbol{\sigma}_2$. No fault contains $\boldsymbol{\sigma}_2$ if the fault patterns are additionally orthorhombic and symmetric about the principal stress axes (Fig. 3b).

The theory of faulting by microcrack linkage along most favourable planes of interaction between mode I cracks (Healy et al. (2006) is a third case in which faults may not contain $\boldsymbol{\sigma}_2$. The theory suggests that poles to faults should be distributed

Fig. 2. Models for the relationships between extension fractures, faults and principal stresses. Extension fractures are black lines (red in the coloured figures), faults or incipient faults are black lines with half arrows, fractures loaded under shear in (b) are grey lines. Left and right columns are early and late stages in fault/fracture evolution respectively. The principal stress vectors are $\boldsymbol{\sigma}_1$, $\boldsymbol{\sigma}_2$, $\boldsymbol{\sigma}_3$, with magnitudes $\sigma_1 \geq \sigma_2 \geq \sigma_3$, taking compression positive. (a) Extension fractures are widespread precursors to faults. The evolution of a fault from an array of extension fractures, as in the Peng and Johnson (1972) beam buckling model, is shown. (b) Extension fractures propagate from flaws loaded in shear to form wing cracks. Incipient linkage of wing cracks in an array is shown to the right (cf. Horii and Nemat-Nasser, 1985). (c) Extension fractures are localised in a fault process zone on a propagating fault. The orientation of extension fractures in the process zone around the fault tips is shown after Vermilye and Scholz (1998). Only the extension fractures in the active process zone are shown in each view. (d) Extension fractures form after slip on faults. "Microscopic feather fractures" are fractures with a characteristic tapered shape, confined to zone adjacent to fault, as shown in black (e.g. Friedman and Logan, 1970). (e) Extension fractures form after slip on faults due to "wavy" fault surface (Chester and Chester, 2000). (f) Extension fractures link with faults to form a fault facture mesh (e.g. Sibson, 1996).

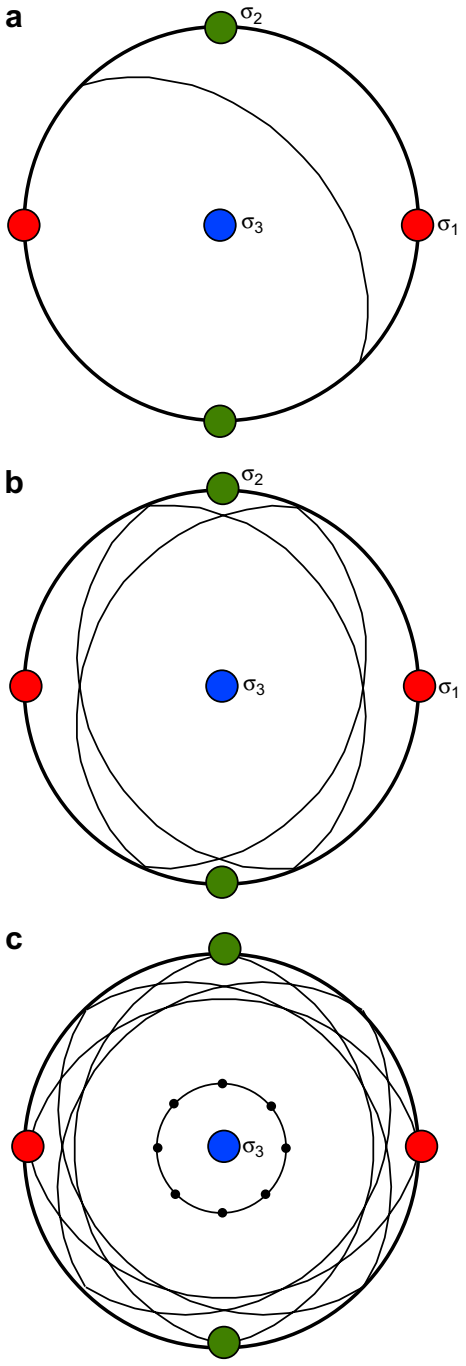

Fig. 3. Faults that do not contain the intermediate principal stress axis. All diagrams are lower hemisphere, equal area stereoplots. (a) Fault plane in an arbitrary orientation with respect to principal stresses due to reactivation. (b) Orthorhombic faults that are symmetrical about the principal stresses. (c) The Healy theory (Healy et al., 2006) for faulting by extension fracture interaction. Poles to fault are distributed on a cone around the local minimum principal stress with an apical angle of 26°. The other principal stresses have no specified orientation with respect to the faults.

on cones with an apical angle of 26° about the local minimum principal stress (Fig. 3c). Fault reactivation, multiple fault sets, and the Healy theory require a more general consideration of the relationship between extension fractures and faults than situations in which faults contain $\boldsymbol{\sigma}_2$.

3. The general relationship between faults, extension fractures, and stresses

The following analysis uses a coordinate framework of principal stress axes $\boldsymbol{\sigma}_1$, $\boldsymbol{\sigma}_2$, $\boldsymbol{\sigma}_3$ in the x, y, and z directions (cf. Jaeger and Cook, 1979; Fig. 4a). The orientation of a fault-plane normal ($\boldsymbol{f}$) is specified by its direction cosines l, m, and n. The direction ratios of maximum resolved shear stress on the fault plane, $\boldsymbol{\tau}$, are given by expression 38 of Jaeger and Cook (1979, p. 22):

$$l\{m^2(\sigma_2-\sigma_1)-n^2(\sigma_1-\sigma_3)\},m\{n^2(\sigma_3-\sigma_2)-l^2(\sigma_2-\sigma_1)\},\\ n\{l^2(\sigma_1-\sigma_3)-m^2(\sigma_3-\sigma_2)\} \quad (1)$$

Following a similar approach to Lisle (2000), and using the stress ratio $\phi = (\sigma_2 - \sigma_3)/(\sigma_1 - \sigma_3)$, Eq. (1) can be simplified by dividing by $-(\sigma_1 - \sigma_3)$ to:

$$l\{m^2(1-\phi)+n^2\},m\{n^2\phi+l^2(\phi-1)\},n\{m^2\phi-l^2\} \quad (2)$$

The line of intersection $\boldsymbol{i}$ between the extension fracture (a plane normal to $\boldsymbol{\sigma}_3$) and the fault plane is called "the fault–

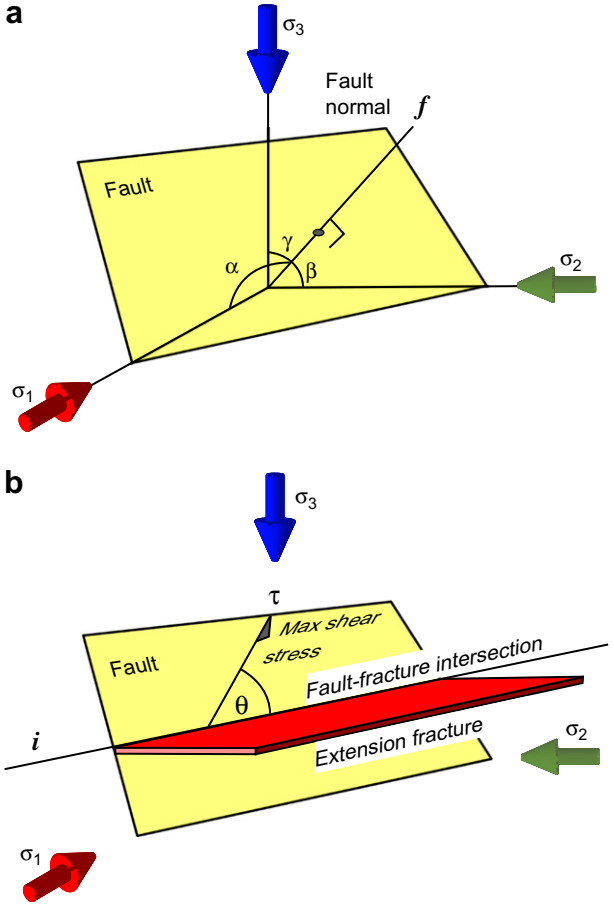

Fig. 4. (a) Coordinate framework for analysis of faults and extension fractures. Principal stresses $\boldsymbol{\sigma}_1$, $\boldsymbol{\sigma}_2$, $\boldsymbol{\sigma}_3$, fault plane normal $\boldsymbol{f}$, specified by angles α, β and γ giving direction cosines l, m, n. (b) An extension fracture with normal in the $\boldsymbol{\sigma}_3$ direction intersects the fault along $\boldsymbol{i}$. The direction of maximum resolved shear stress is $\boldsymbol{\tau}$. The angle between $\boldsymbol{i}$ and τ is θ.

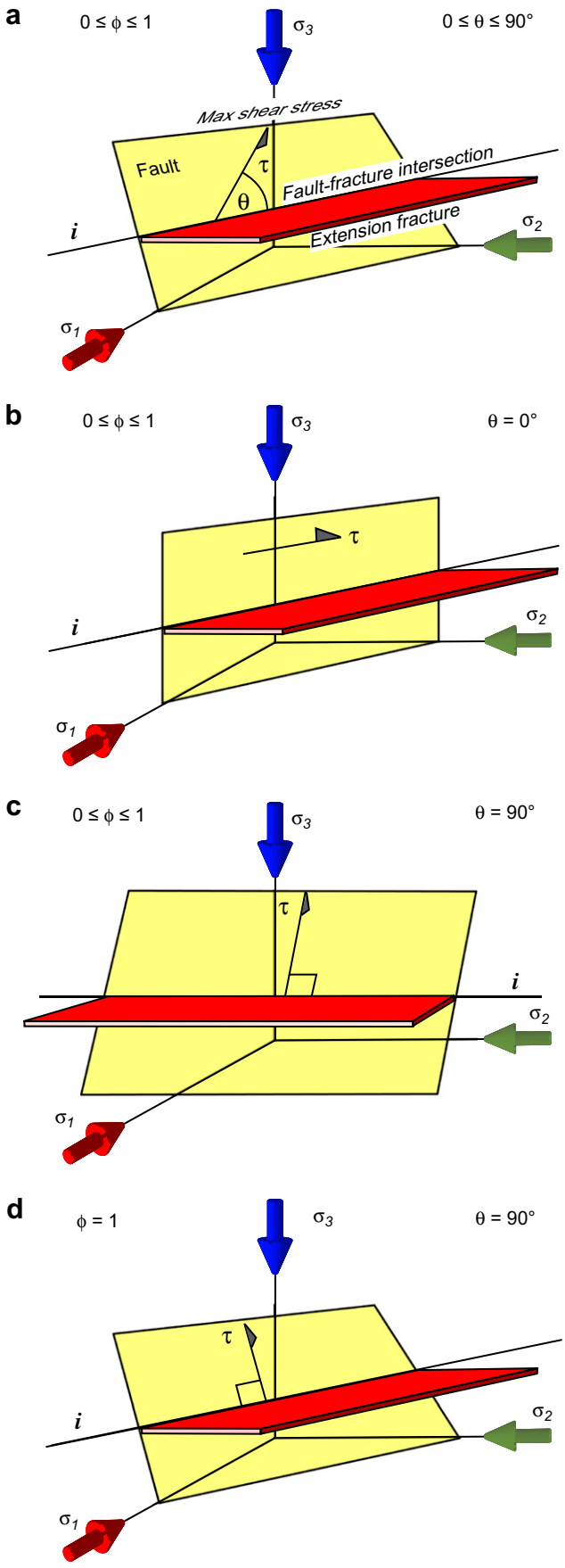

Fig. 5. Results from the general relationship between faults, extension fractures, and principal stresses. $\boldsymbol{i}$ and $\boldsymbol{\tau}$ are as described in Fig. 4. (a) General situation. (b) When the fault plane contains $\boldsymbol{\sigma}_3$, θ is 0° for any value of ϕ. (c) θ is 90° when the fault contains $\boldsymbol{\sigma}_2$. (or $\boldsymbol{\sigma}_1$, not shown) for any value of ϕ. (d) When $\phi = 1$, θ is 90° for any fault orientation.

fracture intersection line'' (Fig. 4b), and is given by the vector or cross product of the fault plane normal $\boldsymbol{f}$, and the normal to the extension fracture, which is the $\boldsymbol{\sigma}_3$ direction with direction ratios (0, 0, 1):

$$\boldsymbol{i} = \boldsymbol{f} \times \boldsymbol{\sigma}_3$$

giving direction ratios $(-m, l, 0)$. The condition for perpendicularity between this line and the direction of maximum resolved shear stress, $\boldsymbol{\tau}$, is:

$$\boldsymbol{\tau i} = 0 \tag{3}$$

which gives:

$$-lm^3(1-\phi) - lmn^2 + lmn^2\phi - l^3m(1-\phi) = ml(\phi - 1) = 0 \tag{4}$$

Eq. (4) is solved when m or l are 0, and when $\phi = 1$. This important result demonstrates that the fault–fracture intersection line will be perpendicular to the direction of maximum resolved shear stress on the fault plane for any fault containing $\boldsymbol{\sigma}_1$ or $\boldsymbol{\sigma}_2$, and for any fault when ϕ is 1, implying that $\sigma_1 = \sigma_2$. For any other fault, i.e. when the fault plane does not contain $\boldsymbol{\sigma}_1$ or $\boldsymbol{\sigma}_2$, and $\phi \neq 1$, extension fractures will not intersect the fault plane perpendicular to the direction of maximum resolved shear stress.

In this more general situation, an angle θ exists between the fault–fracture intersection line $\boldsymbol{i}$, and the direction of maximum resolved shear stress $\boldsymbol{\tau}$. Then Eq. (3) becomes:

$$\boldsymbol{\tau i} = \cos\theta \tag{5}$$

The solution to this equation is more complex because the left hand side must be normalised by the determinant, $\sqrt{k}$, of the direction ratios in Eq. (3):

$$k = \left(l\{m^2(1-\phi) + n^2\}\right)^2 + \left(m\{n^2\phi + l^2(\phi - 1)\}\right)^2 + \left(n\{m^2\phi - l^2\}\right)^2$$

Using Eq. (5) and $n = 1 - l^2 - m^2$ leads to:

$$\cos\theta = \frac{-ml\{m^2(1-\phi) + n^2\}}{\sqrt{k}} + \frac{lm\{n^2\phi + l^2(\phi - 1)\}}{\sqrt{k}} = \frac{ml(\phi - 1)}{\sqrt{k}} \tag{6}$$

This equation shows that the angle θ between $\boldsymbol{\tau}$ and $\boldsymbol{i}$ depends on the stress ratio (ϕ) and the orientation of the fault plane with respect to the principal stresses (given by l, m).

Eq. (6) indicates that $\boldsymbol{i}$ can make variable angles θ with $\boldsymbol{\tau}$ (Fig. 5a), within a range taken from 0° to 90°. Extension fractures intersect the fault plane parallel to $\boldsymbol{\tau}$ (i.e. $\theta = 0°$)

when the fault plane has any orientation that contains $\boldsymbol{\sigma}_3$ (Fig. 5b), and perpendicular to $\boldsymbol{\tau}$ ($\theta = 90°$) when the fault plane contains $\boldsymbol{\sigma}_1$ or $\boldsymbol{\sigma}_2$ (Fig. 5c). When $\phi = 1$, θ is 90° for all fault orientations (Fig. 5d).

For other values of ϕ and fault orientations, θ is distributed in the range 0° to 90°, becoming progressively more evenly distributed through the range as ϕ tends to 0. A histogram of θ values is shown in Fig. 6a from the solution to Eq. (6) for 2000 random values of ϕ and fault plane orientations. The histogram excludes the principal planes of stress in which no slip can occur because they lack shear stress. The histogram shows that 55% of θ values will be 80° or less, indicating that on average an extension fracture will intersect a fault plane at less than 80° to $\boldsymbol{\tau}$ in a random population. The dependence of θ on ϕ is explored further in Figs. 6b and 6c, which show θ values calculated in a similar fashion for $\phi = 0.3$ (approximately the average crustal value: Lisle et al., 2006) and $\phi = 0$. As ϕ decreases, θ values become progressively smaller. For $\phi = 0.3$, 74% of θ values are less than 80°, rising to 86% for $\phi = 0$. These histograms illustrate solutions to Eq. (6), and may differ from the distribution of θ in nature because faults may not be orientated randomly.

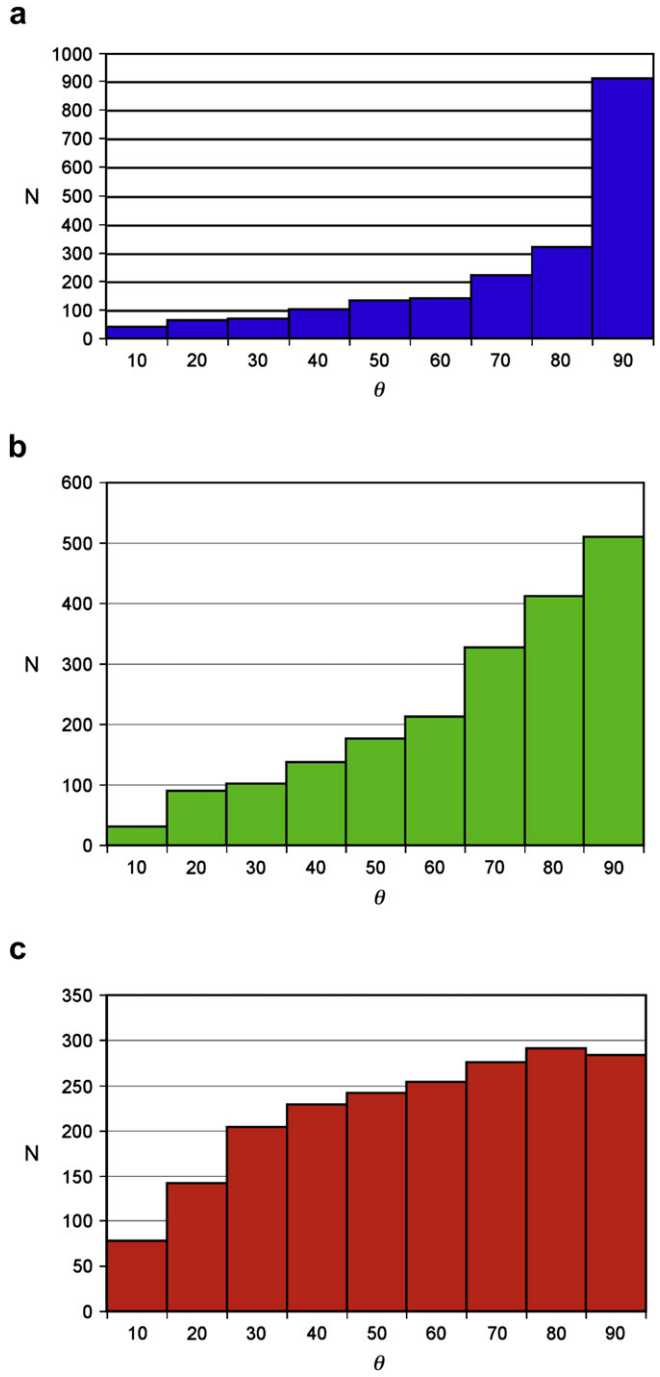

Fig. 6. (a) Histogram of θ for 2000 random fault orientations and ϕ values ($0 \leq \phi \leq 1$), calculated from Eq. (6). (b) Histogram of θ for $\phi = 0.3$, the average crustal value, and 2000 random fault orientations. (c) Histogram of θ for $\phi = 0$, and 2000 random fault orientations.

4. Field examples of oblique relationships between fault–fracture intersection lines and related fault slip vectors

Many field examples show extension fractures intersecting faults perpendicular to the slip direction (e.g. Sibson et al., 1988; de Ronde et al., 2001; Wilkins et al., 2001; Miller and Wilson, 2004). However, other studies show different relationships. The following examples are selected according to the criteria that (1) extension fractures and faults are spatially associated, (2) they are reasonably inferred to belong to the same deformation event, and (3) orientations of planar and linear features that can be estimated to an accuracy of 2° or better.

The Larra thrust is a bedding-parallel thrust in the southern Pyrenees, described by Teixell et al. (2000). The thrust formed in the middle Eocene at 6–7 km depth in anchizonal-lowermost greenschist facies conditions, and has a displacement of 5 km. Within the study area, the thrust is developed along the contact of two limestones, with generally south to southwest transport directions. At the Pierre-Saint-Martin locality, a detailed section of the decollement contains intense bedding parallel veining and oblique extension veins. Table 2 shows that the vector mean of θ measurements for six of these veins (relative to the southwest trending thrust lineation) is $66 \pm 17°$ (95% confidence intervals are quoted).

A second example of veins related to a thrust is described in the northern Appalachians in Maine near Allagash (Bradley and Bradley, 1994), where the Walker Brook duplex formed during Acadian deformation under lower greenschist facies. The duplex is developed in a single turbidite bed 1 m thick of very fine sandstone to mudstone, and has a displacement of 185 m. The original transport direction was to the west in sinistral-reverse movement. Quartz extension veins formed during thrusting. A mean vein orientation from approximately 50 vein measurements gives a θ value of 62° (Table 2; no confidence interval because measurements were grouped).

The Bayas fault in the Cantabrian Zone of the Ibero-Armorican arc in North Spain provides a strike–slip example (Blenkinsop and Drury, 1988). The strike–slip deformation occurred in the Westphalian under a maximum stratigraphic depth of burial of 4 km, at temperatures of 148–248 °C. Veins of quartz, barite and iron oxides occur adjacent to the fault

Table 2
θ values (vector means) from three field examples where θ is less than 90°

Location	Rock types	Fault	θ	κ	95% CI	N	Reference
Pyrenees 0°46′ E 42°58′ N	Limestone	Larra Thrust Fault	66	7.5	17	6	Teixell et al. (2000)
Appalachians 69°08′ W 47°07′ N	Sandstone–mudstone	Walker Brook Thrust Duplex	62			~50	Bradley and Bradley (1994)
Ibero-Armorican Arc 6°2′ W 43°40′ N	Quartzite	Bayas Strike Slip Fault	52	13.4	9	11	Blenkinsop and Drury (1988)

κ, concentration parameter of the Von Mises distribution (calculated after Piazolo and Passchier, 2002); CI, confidence interval (°); N, number of extension fractures.

within the Barrios Formation, a fine-medium grained quartzite. Dextral oblique displacement on the Bayas fault was accompanied by opening of the veins since they are partly filled with cataclasite from the fault plane. The vector mean of 11 vein measurements gives a θ value of $52 \pm 11°$, measured relative to the lineations and corrugations of the fault surface that plunge 28° NE (Table 2).

5. Discussion

A number of careful field observations demonstrate that θ values can differ from 90° by amounts that are well outside observational error and the confidence intervals on the data. These observations are consistent with the theoretical analysis above. The analysis is given in the context of the direction of maximum resolved shear stress on a fault. The applicability of the analysis therefore depends on the extent to which faults obey the Wallace–Bott criterion that slip on faults occurs in the direction of maximum resolved shear stress (Wallace, 1951; Bott, 1959). The few attempts that have been made to verify the Wallace–Bott hypothesis against independent criterion either directly (Lisle and Srivastava, 2004) or indirectly by demonstrating the validity of dynamic analysis (e.g. Blenkinsop, 2006), suggest that the hypothesis is generally correct.

Fault slip or fault interaction may perturb stress around faults. Several field and modelling studies have investigated these effects (e.g. Sassi and Faure, 1997; Kattenhorn et al., 2000; Bourne and Willemse, 2001; Maerten et al., 2002; Roberts, 2007). The perturbing effects of slip can be identified because they are intensified at fault tips (e.g. Kattenhorn et al., 2000; Roberts, 2007), and effects due to fault interaction should be recognisable from the relation between secondary structures and fault distribution (e.g. Maerten et al., 2002). The relationship between stress, fault and fracture orientations derived above will still be valid for the perturbed stress state if slip occurs according to the Wallace–Bott criterion.

A comprehensive study to further test the applicability of the theory should be a goal for future research. Such a study would require orientations and relative values of principal stresses to be obtained independently from the orientations of the extension fractures, as well as demonstrating that extension fractures can be clearly linked to faulting. Dynamic analysis by the inversion of fault slip data (e.g. Angelier, 1984; Lisle, 1988; Ramsay and Lisle, 2000; Lisle et al., 2006) would be one way to obtain the stresses. Alternatively borehole data in an area of active faulting might be used (e.g. Chester et al., 2007; Hickman et al., 2007; Zoback et al., 2007). In both cases, the possibility of stress perturbation may place limits on the scale of the analysis.

The theory and field data have some significant implications for the use of extension fractures in kinematic and dynamic analysis. The most simple consequence of the field examples is that θ should not be assumed to be 90°. However, this value is likely if the fault plane can be demonstrated to contain $\boldsymbol{\sigma}_2$ (for example, by conjugate faults, e.g. de Ronde et al., 2001), or if the value of ϕ is 1. Extension fractures can also be used in dynamic analysis through Eq. (6), which allows the value of ϕ to be calculated given known orientations of principal stresses relative to the fault planes, and the orientation of fault- fracture intersection line.

6. Conclusions

Most models that account for the common association between extension fractures and faults deal with extension fractures that form prior to, during or after fault propagation in the same deformation event, and assume that faults contain the intermediate principal stress axis. Extension fractures intersect faults along lines perpendicular to the slip direction in these models. However, at least three types of faults may not contain the intermediate principal stress: reactivated faults, faults in multiple sets, and Healy theory faults (Healy et al., 2006). These circumstances require consideration of a more general relationship between faults, extension veins/fractures and stresses.

Theoretical analysis shows that the angle θ between the fault–fracture intersection line and the direction of maximum resolved shear stress on a fault plane can range from 0° to 90°. This angle depends on the orientation of the fault plane with respect to the principal stresses, as well as the ratios between the principal stresses. Extension fractures will only intersect the fault plane perpendicular to the direction of maximum resolved shear stress when the fault plane contains $\boldsymbol{\sigma}_1$ or $\boldsymbol{\sigma}_2$ (the latter is the case for most fault propagation models), or when the value of $\phi = (\sigma_2 - \sigma_3)/(\sigma_1 - \sigma_3) = 1$, indicating

that $\sigma_1 = \sigma_2$. In cases where the fault plane contains $\boldsymbol{\sigma}_3$, extension fractures can intersect the fault plane parallel to the direction of maximum resolved shear stress.

Field examples support the contention of the analysis that values of θ may differ significantly from 90°. Such oblique values of θ may be indicators of fault reactivation, multiple sets of faults, or Healy theory faults. Fault slip vectors and intersections with extension fractures should be measured separately in the field, and should not be assumed as perpendicular.

Acknowledgements

Julie Graham, Gustav Nortje, and Nick Oliver are thanked for discussion, and Rick Sibson for pointing out the locality in Fig. 1. The reviewers David Peacock and Scot Wilkins made useful and constructive reviews, and the editor Bill Dunne helped to improve the manuscript.

References

Acocella, V., Korme, T., Salvini, F., 2003. Formation of normal faults along the axial zone of the Ethiopian Rift. Journal of Structural Geology 25, 503–513.

Anders, M.H., Wiltschko, D.V., 1994. Microfracturing, paleostress and the growth of faults. Journal of Structural Geology 16, 795–815.

Angelier, J., 1984. Tectonic analysis of fault slip data sets. Journal of Geophysical Research 89, 5835–5848.

Aydin, A., Reches, Z., 1982. Number and orientation of fault sets in the field and in experiments. Geology 10, 107–112.

Beacom, L.E., Anderson, T.B., Holdsworth, R.E., 1999. Using basement-hosted clastic dykes as syn-rifting palaeostress indicators: an example from the basal Stoer group, northwest Scotland. Geological Magazine 136, 301–310.

Blenkinsop, T.G., 2006. Kinematic and dynamic fault slip analyses: implications from the surface rupture of the 1999 Chi-Chi, Taiwan, earthquake. Journal of Structural Geology 28, 1040–1050.

Blenkinsop, T.G., Drury, M., 1988. Stress estimates and fault history from quartz microstructures. Journal of Structural Geology 10, 673–684.

Blenkinsop, T.G., Rutter, E.H., 1986. Cataclastic deformation of a quartzite in the Moine thrust zone. Journal of Structural Geology 8, 669–681.

Bott, M.H.P., 1959. The mechanics of oblique slip faulting. Geological Magazine 96, 109–117.

Brace, W.E., Bombolakis, E.G., 1963. A note on brittle crack growth in compression. Journal of Geophysical Research 68, 3709–3713.

Brace, W.F., Martin, R.J., 1968. A test of the effective stress law for crystalline rocks of low porosity. International Journal of Rock Mechanics and Mining Science 5, 415–426.

Brace, W.F., Paulding, B.W., Scholz, C., 1966. Dilatancy in the fracture of crystalline rocks. Journal of Geophysical Research 71, 3939–3941.

Bradley, D.C., Bradley, L.M., 1994. Geometry of an outcrop-scale duplex in Devonian flysch, Maine. Journal of Structural Geology 16, 371–380.

Bourne, S.J., Willemse, E.J.M., 2001. Elastic stress control on the pattern of tensile fracturing around a small fault network at Nash Point, U.K. Journal of Structural Geology 23, 1753–1770.

Chester, F.M., Chester, J.S., 2000. Stress and deformation along wavy frictional faults. Journal of Geophysical Research 105, 23421–23430.

Chester, J.S., Fletcher, R., 1997. Stress distribution and failure in anisotropic rock near a bend on a weak fault. Journal of Geophysical Research 102, 693–708.

Chester, J.S., Chester, F.M., Kirschner, D.L., Almeida, R., Evans, J.P., Guillemette, R.N., Hickman, S., Zoback, M., Ellsworth, W., 2007. Deformation of sedimentary rock across the San Andreas Fault Zone: Mesoscale and microscale structures displayed in core from SAFOD. Eos, Transactions of the American Geophysical Union. 88(52), Fall Meeting Supplement, Abstract T42C-05.

Conrad, R.E., Friedman, M., 1976. Microscopic feather fractures in the faulting process. Tectonophysics 33, 187–198.

Cooke, M.L., 1997. Fracture localization along faults with spatially varying friction. Journal of Geophysical Research 102, 22425–22434.

Cowie, P.A., Scholz, C.H., 1998. Physical explanation for the displacement-length relationship of faults using a post-yield fracture mechanics model. Journal of Structural Geology 14, 1133–1148.

Cox, S.J.D., Scholz, C.H., 1988. On the formation and growth of faults: An experimental study. Journal of Structural Geology 10, 413–430.

Crider, J.G., 2001. Oblique slip and the geometry of normal-fault linkage: mechanics and a case study from the Basin and Range in Oregon. Journal of Structural Geology 23, 1997–2009.

Crider, J.G., Peacock, D.C.P., 2004. Initiation of brittle faults in the upper crust: a review of field observations. Journal of Structural Geology 26, 691–707.

Cruikshank, K.M., Zhao, G., Johnson, A.M., 1991. Analysis of minor fractures associated with joints and faulted joints. Journal of Structural Geology 13, 865–886.

De Paola, N., Holdsworth, R.E., McCaffrey, K.J.W., 2005. The influence of lithology and pre-existing structures on reservoir-scale faulting patterns in transtensional rift zones. Journal of the Geological Society of London 162, 471–480.

de Ronde, C.E.J., Sibson, R.H., Bray, C.J., Faure, K., 2001. Fluid chemistry of veining associated with an ancient microearthquake swarm, Benmore Dam. New Zealand. Bulletin of the Geological Society of America 113, 1010–1024.

Eichhubl, P., Boles, J.R., 2000. Focused fluid flow along faults in the Monterey Formation, coastal California. Bulletin of the Geological Society of America 112, 1667–1679.

Engelder, J.T., 1974. Cataclasis and the generation of fault gouge. Bulletin of the Geological Society of America 85, 1515–1522.

Engelder, J.T., 1989. The analysis of pinnate joints in the Mount Desert island granite: implications for post intrusion kinematics in the coastal belt, Maine. Geology 17, 564–567.

Friedman, M., Logan, J.M., 1970. Microscopic Feather Fractures. Bulletin of the Geological Society of America 81, 3417–3420.

Granier, T., 1985. Origin, damping, and pattern of development of faults in granite. Tectonics 4, 721–737.

Hancock, P.L., Barka, A.A., 1987. Kinematic indicators on active normal faults in western Turkey. Journal of Structural Geology 9, 573–584.

Healy, D., Jones, R.R., Holdsworth, R.E., 2006. Three-dimensional brittle shear fracturing by tensile crack interaction. Nature 439, 64–67, doi:10.1038/nature04346.

Hickman, S., Zoback, M., Ellsworth, W., Kirschner, D., Solum, J., 2007. Structure and composition of the San Andreas Fault at seismogenic depths: Recent results from the SAFOD experiment. Eos, Transactions of the American Geophysical Union, 88(52), Fall Meeting Supplement, abstract T44B-01.

Hill, D.P., 1977. A model for earthquake swarms. Journal of Geophysical Research 82, 347–352.

Horii, H., Nemat-Nasser, S., 1985. Compression-induced microcrack growth in brittle solids: axial splitting and shear failure. Journal of Geophysical Research 90, 3105–3125.

Imber, J., Holdsworth, R.E., McCaffrey, K.J.W., Wilson, R.W., Jones, R.R., England, R.W., Gjeldvik, G., 2005. Early Tertiary sinistral transpression and fault reactivation in the western Vøring basin, Norwegian Sea: Implications for hydrocarbon exploration and pre-breakup deformation in ocean margin basins. American Association of Petroleum Geologists Bulletin 89, 1043–1069.

Jaeger, J.C., Cook, N.G.W., 1979. Fundamentals of Rock Mechanics, (third ed.). Chapman and Hall, London.

Johnson, A.M., 1995. Orientations of faults determined by premonitory shear zones. Tectonophysics 247, 161–238.

Jones, R.R., Holdsworth, R.E., McCaffrey, K.J.W., Clegg, P., Tavarnelli, E., 2005. Scale dependence, strain compatibility and heterogeneity of three-dimensional deformation during mountain building: a discussion. Journal of Structural Geology 27, 1190–1204.

Kattenhorn, S.A., Marshall, S.T., 2006. Fault-induced perturbed stress fields and associated tensile and compressive deformation at fault tips in the ice shell of Europa: implications for fault mechanics. Journal of Structural Geology 28, 2204–2221.

Kattenhorn, S.A., Aydin, A., Pollard, D.D., 2000. Joins at high angles to normal fault strike: an explanation using 3-D numerical models of fault-perturbed stress fields. Journal of Structural Geology 22, 1–23.

Kemeny, J.M., Cook, N.G.W., 1987. Crack models for the failure of rocks in compression, in: 2nd International Conference on Constitutive Laws for Engineering Materials, Tucson, p. 879–887.

Krantz, R.W., 1988. Multiple fault sets and three-dimensional strain: theory and application. Journal of Structural Geology 10, 225–238.

Lafrance, B., 2004. Conjugate oblique-extension veins in shear and tensile fracture systems at the Komis gold mine and Mufferaw gold prospect, northern Saskatchewan. Exploration Mining Geology 13, 129–137.

Lawn, B.R., Wilshaw, T.R., 1975. Fracture of Brittle Solids. Cambridge University Press, Cambridge.

Lisle, R.J., 1988. Romsa: a Basic program for palaeostress analysis using fault-striation data. Computers & Geosciences 14, 255–259.

Lisle, R.J., Srivastava, D.C., 2004. Test of the frictional reactivation theory for faults and validity of fault-slip analysis. Geology 32, 569–572.

Lisle, R.J., Orife, T.O., Arlegui, L., Liesa, C., Srivastava, D.C., 2006. Favoured states of palaeostress in the Earth's crust: evidence from fault-slip data. Journal of Structural Geology 28, 1051–1066.

Maerten, L., Gillespie, P., Pollard, D.D., 2002. Effects of local stress perturbation on secondary fault development. Journal of Structural Geology 24, 145–153.

Martel, S., 1990. Formation of compound strike-slip fault zones, Mount Abbot quadrangle, California. Journal of Structural Geology 212, 869–877.

Martel, S.J., Langley, J.S., 2006. Propagation of normal faults to the surface in basalt, Koae fault system, Hawaii. Journal of Structural Geology 28, 2123–2143.

Martel, S.J., Pollard, D.D., Segall, P., 1988. Development of simple strike-slip fault zones, Mount Abbot Quadrangle, Sierra Nevada, California. Bulletin of the Geological Society of America 100, 1451–1465.

McEwen, T.J., 1981. Brittle deformation in pitted pebble conglomerates. Journal of Structural Geology 3, 25–37.

Miller, J.McL., Wilson, C.J.L., 2004. Structural analysis of faults related to a heterogeneous stress history: reconstruction of a dismembered gold deposit, Stawell, western Lachlan Fold Belt, Australia. Journal of Structural Geology 26, 1231–1256.

Miller, J.McL., Nelson, E.P., Hitzman, M., Muccilli, P., Hall, W.D.M., 2007. Orthorhombic fault-fracture patterns and non-plane strain in a synthetic transfer zone during rifting: Lennard shelf, Canning basin, Western Australia. Journal of Structural Geology 29, 1002–1021.

Mollema, P.N., Antonellini, M., 1999. Development of strike-slip faults in the dolomites of the Sella Group, Northern Italy. Journal of Structural Geology 21, 273–292.

Oertel, G., 1965. The mechanism of faulting in clay experiments. Tectonophysics 2, 343–393.

Oesterlen, P., Blenkinsop, T.G., 1995. Extension directions and strain near the failed triple junction of the Zambezi and Luangwa rift zones, southern Africa. Journal of African Earth Sciences 18, 175–180.

Olson, J.E., Pollard, D.D., 1991. The initiation and growth of en échelon veins. Journal of Structural Geology 10, 445–452.

Paterson, M.S., 1978. Experimental Rock Deformation: The Brittle Field. Springer, Berlin.

Peacock, D.C.P., Sanderson, D.J., 1992. Effects of layering and anisotropy on fault geometry. Journal of the Geological Society of London 149, 793–802.

Peacock, D.C.P., Sanderson, D.J., 1995a. Pull-aparts, shear fractures and pressure solution. Tectonophysics 241, 1–13.

Peacock, D.C.P., Sanderson, D.J., 1995b. Strike-slip relay ramps. Journal of Structural Geology 17, 1351–1360.

Peng, S., Johnson, A.M., 1972. Crack growth and faulting in a cylindrical sample of Chelmsford Granite. International Journal of Rock Mechanics and Mining Science 9, 37–86.

Petit, J.P., Barquins, M., 1988. Can natural faults propagate under Mode II conditions? Tectonics 7, 1243–1256.

Piazolo, S., Passchier, C.W., 2002. Controls on lineation development in low to medium grade shear zones: a study from the Cap de Creus peninsula, NE Spain. Journal of Structural Geology 24, 25–44.

Pollard, D.D., Segall, P., 1987. Theoretical displacements and stresses near fractures in rock: with applications to faults, joints, veins, dikes, and solution surfaces. In: Atkinson, B.K. (Ed.), Fracture Mechanics of Rock. Academic Press, London, pp. 277–349.

Ramsay, J.G., Lisle, R.J., 2000. The Techniques of Modern Structural Geology. In: Applications of Continuum Mechanics in Structural Geology, Vol. 3. Academic Press, London.

Reches, Z., 1978. Analysis of faulting in a three-dimensional strain field. Tectonophysics 47, 109–129.

Reches, Z., 1983. Faulting of rocks in three-dimensional strain fields II. Theoretical analysis. Tectonophysics 95, 133–156.

Reches, Z., Dietrich, J.H., 1983. Faulting of rocks in three dimensional strain fields I. Failure of rocks in polyaxial, servocontrolled experiments. Tectonophysics 95, 111–132.

Reches, Z., Lockner, D.A., 1994. Nucleation and growth of faults in brittle rocks. Journal of Geophysical Research 99, 18159–18174.

Rispoli, R., 1981. Stress fields about strike-slip faults inferred from stylolites and tension gashes. Tectonophysics 75, T29–T36.

Roberts, G.P., 2007. Fault orientation variations along the strike of active normal fault systems in Italy and Greece: Implications for predicting the orientations of subseismic-resolution faults in hydrocarbon reservoirs. Bulletin of the American Association of Petroleum Geologists 91, 1–20.

Rudnicki, J.W., 1980. Fracture mechanics applied to the Earth's crust. Annual Reviews of Earth and Planetary Science 8, 489–525.

Rutter, E.H., Hadizadeh, J., 1991. On the influence of porosity on the low-temperature brittle-ductile transition in siliciclastic rocks. Journal of Structural Geology 13, 609–614.

Sassi, W., Faure, J.-L., 1997. Role of faults and layer interfaces on the spatial variation of stress regimes in basins: inferences from numerical modeling. Tectonophysics 266, 101–119.

Scholz, C.H., 1968. Microfracturing and the inelastic deformation of rock in compression. Journal of Geophysical Research 73, 1417–1432.

Scholz, C.H., Dawers, N.H., Yu, Z., Anders, M.H., Cowie, P.H., 1993. Fault growth and scaling laws: Preliminary results. Journal of Geophysical Research 98, 21951–21961.

Segall, P., Pollard, D.D., 1983. Nucleation and growth of strike slip faults in granite. Journal of Geophysical Research 88, 555–568.

Shipton, Z.K., Cowie, P.A., 2001. Fault tip displacement gradients and process zone dimensions. Journal of Structural Geology 20, 983–997.

Sibson, R.H., 1996. Structural permeability of fluid-driven fault-fracture meshes. Journal of Structural Geology 18, 1031–1042.

Sibson, R.H., 2004. Controls on maximum fluid overpressure defining conditions for mesozonal mineralization. Journal of Structural Geology 26, 1127–1136.

Sibson, R.H., Robert, F., Poulsen, H., 1988. High angle reverse faults, fluid pressure cycling and mesothermal gold-quartz deposits. Geology 16, 551–555.

Smith, J.V., 1996. En Echelon sigmoidal vein arrays hosted by faults. Journal of Structural Geology 18, 1173–1179.

Tapponier, P., Brace, W.F., 1976. Development of stress induced microcracks in Westerly granite. International Journal of Rock Mechanics and Mining Science & Geomechanics Abstracts 13, 103–112.

Teixell, A., Durney, D.W., Arboley, M.-L., 2000. Stress and fluid control on decollement within competent limestone. Journal of Structural Geology 22, 349–371.

Teufel, L.W., 1981. Pore volume changes during frictional sliding of simulated faults. In: Carter, N.L., Friedman, M., Logan, J.M., Stearns, D.W. (Eds.), Mechanical Behaviour of Crustal RockAmerican Geophysical Union Geophysical Monograph 24, pp. 135–145.

Tunks, A.J., Selley, D., Rogers, J.R., Brabham, G., 2004. Vein mineralization at the Damang Gold Mine, Ghana: controls on mineralization. Journal of Structural Geology 26, 1257–1273.

Vermilye, J.M., Scholz, C.H., 1998. The process zone: a microstructural view of fault growth. Journal of Geophysical Research 103, 12223–12237.

Wallace, R.E., 1951. Geometry of shearing stress and relation to faulting. Journal of Geology 59, 118–130.

Wilkins, S.J., Gross, M.R., Wacker, M., Eyal, Y., Engelder, T., 2001. Faulted joints: kinematics, displacement-length scaling relations and criteria for their identification. Journal of Structural Geology 23, 315–327.

Willemse, E.J.M., Pollard, D.D., 1998. On the orientation and patterns of wing cracks and solution surfaces at the tips of a sliding flaw or fault. Journal of Geophysical Research 103, 2427–2438.

Willemse, E.J.M., Peacock, D.C.P., Aydin, A., 1997. Nucleation and growth of strike-slip faults in limestones from Somerset, UK. Journal of Structural Geology 19, 1461–1477.

Wilson, J.E., Chester, J.S., Chester, F.M., 2003. Microfracture analysis of fault growth and wear processes, Punchbowl Fault, San Andreas system, California. Journal of Structural Geology 25, 1855–1873.

Zoback, M.D., Hickman, S.H., Ellsworth, W., Kirschner, D., Pennell, N.B., Chery, J., Sobolev, S., 2007. Preliminary Results from SAFOD Phase 3: Implications for the state of stress and shear localization in and near the San Andreas Fault at depth in central California. Eos, Transactions of the American Geophysical Union, 88(52), Fall Meeting Supplement, Abstract T13G-03.